

# Integrating Multispectral Hemodynamic Imaging for Bulk Tissue Oxygenation Analysis

Megan Y Tran<sup>1</sup>

Robert Amelard<sup>1,2</sup>

Alexander Wong<sup>1,2</sup>

<sup>1</sup>University of Waterloo, Waterloo, Canada

<sup>2</sup>Schlegel-UW Research Institute for Aging, Waterloo, Canada

## Abstract

Tissue perfusion and oxygenation are important factors in predicting patient outcomes, but current non-invasive devices for this type of measurement are limited to contact-based single-site monitoring. We present the co-integration of a multispectral optical-electronic subsystem into an existing non-contact coded hemodynamic imaging (CHI) device to enable image acquisition under different illuminants for spatial tissue oxygenation. Stability of the optical output for three illuminants over 10 mins was validated by the imaging system, with  $\sigma_{\max}=0.407$  intensity units, reflecting stability in local fluctuations, and a maximal overall change of 3.1 units. Bulk tissue oxygenation measurement of the thenar eminence during a cuff occlusion experiment revealed relative changes in absorbance due to oxy- and deoxyhemoglobin consistent with concurrent physiological changes in chromophore concentration as described in a previous study.

## 1. Introduction

Changes in blood and tissue hemodynamics are an important physiological parameter in the assessment of vascular and tissue health. In acute medical care, it is well established that outcomes for high-risk surgical and trauma patients are related to cardiac index and tissue oxygen delivery [1, 2]. Changes in blood perfusion and flow are also important markers for other high-risk groups such as the elderly and infants in neonatal care. In clinical practice, blood flow, perfusion, and oxygenation are inferred by common cardiac parameters such as blood pressure, heart rate, and pulse oximetry, by transcutaneous oxygen measurements [2, 3], or through injected dyes for visual assessment, making it difficult to assess blood hemodynamics. Near infrared (NIR) and diffuse reflectance spectroscopy have previously been demonstrated as feasible methods for quantifying hemoglobin properties [2], but are limited to contact-based single-site monitoring [3, 4]. A recently introduced, non-contact coded hemodynamic imaging (CHI) system has enabled wide-field examination of arterial and venous blood flow [5, 6], and an augmented system enabled thermal information to be captured simultaneously [7]. However, this system is limited to data captured with a single illuminant at a time, rendering it unable to obtain spatial tissue oxygenation data.

To address this, we extend the CHI system to enable multispectral data acquisition with the goal of simultaneously assessing spatiotemporal blood flow and tissue oxygenation. Together, these can provide powerful clinical insights enabling advanced tissue health monitoring. This paper describes the design, integration, and evaluation of an optical light system with electronic switching to achieve stable illumination for the multispectral biophotonic imaging system, as well as electronic design to enable multimodal, plug-and-play flexibility in the optical subsystem. The stability of the optical output was

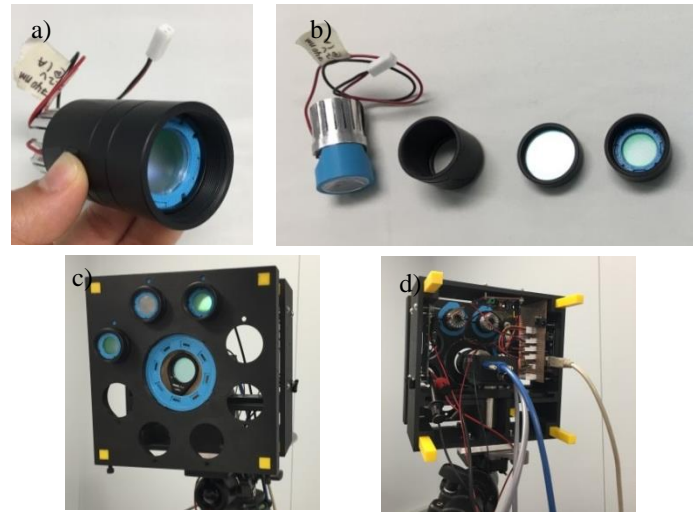


Fig. 1: a) Optical assembly and b) internal optical components. c) Front view of housing, 3 optical assemblies arranged above the camera opening, covered by a linear polarizer. d) Rear of housing, including camera, Arduino, custom circuit and constant-current driver.

validated using through temporal analysis of the captured light intensity and we demonstrate the ability of the multispectral data to show changes in absorbance caused by changes in oxy- and deoxyhemoglobin in the thenar region.

## 2. Methods

The proposed imaging system co-integrates three subsystems: optical, electronic, and computational processing, described in the sections below, where each contribute to the acquisition and processing of the multispectral data. The optical and electronic subsystems were designed to fulfill three main functions: (1) temporally and spatially stable illumination, (2) enabling multispectral imaging through synchronization with the camera, and (3) interchangeability of optical components and illuminants.

### 2.1 Optical subsystem

The optical subsystem was developed with the goal of illuminating the imaging area with spatially homogeneous light. To achieve multispectrality, three systematically selected high-powered LEDs (LEDEngin) with specific peak wavelengths of light in the FR and NIR range (740nm, 850nm, and 940nm) were chosen as the illuminants, which provide illumination on either side of the oxy-deoxyhemoglobin isosbestic point (805nm). The optical assembly shown in Fig. 1a consists of a custom heat sink, LED, lens, lens tube, and fly's-eye condenser, pictured in an exploded view in Fig. 1b. The fly's-eye condenser and heat sink enabled spatially and temporally even illumination, homogeneously diffusing the light over an area and mitigating variance in LED intensity caused by heating, respectively. The images were captured by a CMOS camera with sensitivity in the NIR range (PointGrey GS3-U3-41C6NIR), shown in Fig. 1c and Fig. 1d positioned in the centre of the housing behind a linear polarizer with the three equidistant optical assemblies.

## 2.2 Electronic subsystem

Electronic circuitry synchronized the acquisition and illumination subsystems. Since LED output depends on the amount of current supplied, power is supplied by a constant-current driver (Texas Instruments LM3141HV, PSOP8 evaluation board) to mitigate current-driven fluctuations in light intensity.

In the acquisition of data, the illumination of the three LEDs was time multiplexed synchronously with sequential frame exposures. With the addition of an ambient frame, four videos illuminated with different wavelengths of light were acquired sequentially. The LED switching and camera triggering were controlled externally by a microcontroller via a custom switching circuit that utilized MOSFETs, and powered by the constant-current driver. The circuit can easily be expanded to accommodate additional illuminants and is limited only by the number of digital control pins on the microcontroller. As seen in Fig. 1d, the use of crimped header connectors permits the LED assemblies to be interchanged in the circuit and housing in a plug-and-play style, enabling the device to be used in a variety of modalities.

## 2.3 Hemoglobin absorption estimation

Using this optical-electronic subsystem framework, multispectral imaging can be used to quantitatively assess relative oxy- and deoxyhemoglobin concentration dynamics. A computational biophotonic processing model was used based on the Beer-Lambert law of light attenuation [8]:

$$A(\lambda) = -\log\left(\frac{I^\lambda}{I_0^\lambda}\right) = c_{HbO_2} l_{HbO_2}^\lambda \varepsilon_{HbO_2}^\lambda + c_{Hb} l_{Hb}^\lambda \varepsilon_{Hb}^\lambda \quad (1)$$

where  $A(\lambda)$  is the absorbance at wavelength  $\lambda$ ,  $I$  and  $I_0$  are the transmitted and incident illumination,  $(c, l, \varepsilon)$  are the chromophore concentration, photon path length, and extinction coefficient respectively for oxyhemoglobin, and deoxyhemoglobin.  $I_0$  was determined through white reflectance target calibration. Combining  $c$  and  $l$  into a single chromophore absorption parameter, relative dynamic oxy- and deoxyhemoglobin concentrations were estimated through linear least-squares optimization estimation:

$$\begin{bmatrix} \hat{c}_{Hb} \\ \hat{c}_{HbO_2} \end{bmatrix} = \operatorname{argmin}_c \| \mathbf{a} - \mathbf{X}\mathbf{c} \|^2 \quad (2)$$

where  $\mathbf{a}$  is the observed absorbance vector,  $\mathbf{X}$  is a matrix of relevant spectral extinction coefficients, and  $\mathbf{c}$  is estimated relative chromophore concentrations. These relative concentrations were estimated over a region of interest to provide mean bulk tissue oxygenation.

## 3. Results

### 3.1 Evaluation of optical stability

To assess the temporal stability of the light, the device was positioned 1 m away from a reflectance plane under ambient fluorescent lighting conditions, and two 3-minute videos at 60 fps were captured with the camera over 10 minutes. Both sets of resulting frames are processed into four videos each of 2700

Wavelength (nm)	Time range (mins)	Standard Deviation (pixel intensity units)
740	0-3	0.176
	7-10	0.117
850	0-3	0.437
	7-10	0.210
940	0-3	0.407
	7-10	0.186
Ambient	0-3	0.143
	7-10	0.118

Table 1: Quantification of LED optical stability in a region of interest in terms of standard deviation and variance. For all light sources, only small deviations from the mean occur over time.

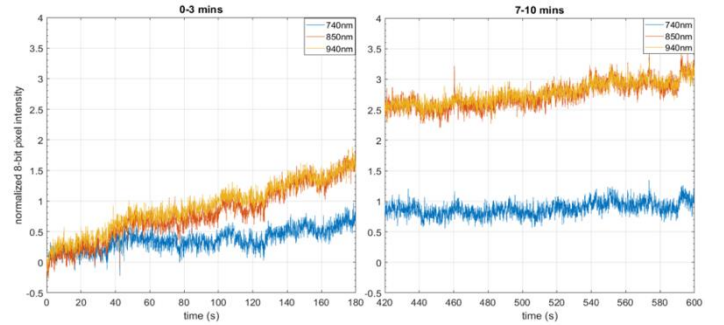


Fig. 2: Graphs of mean pixel intensity plotted from 0-3 mins and 7-10 mins of the 740nm, 850nm, and 940nm LEDs. Each of the LEDs show an increase in intensity from 0-3 mins of no more than 2 units, but this stabilizes in minutes 7-10. Local fluctuations are no more than 0.5 units.

frames, and the mean pixel intensity for each wavelength over time was calculated.

A region of interest in the frames at which the three LED projections overlapped was chosen for the optical stability analysis. Fig. 2 shows the normalized mean 8-bit intensity of the selected region from 0-3 mins (left) and 7-10 mins (right) for each wavelength. Local fluctuations in pixel intensity varied by less than half of a unit, which was reflected in the standard deviations (Table 1), whereas a maximum long-term increase of 3.1 units over 10 minutes in the 940nm LED was observed.

### 3.2 Hemoglobin estimation

Hemoglobin estimation was assessed using an arterial cuff occlusion study. A sphygmomanometer was used on the upper arm to occlude arterial flow by inducing a pressure of 180mmHg. After 45s of occlusion, the cuff pressure was released, re-enabling arterial and venous flow. Multispectral imaging was recorded during this time, and processed according to the biophotonic model from Section 2.3. Fig. 3 shows the results of the chromophore estimations across the region spanning the thenar eminence. Following arterial occlusion (first dotted line), there is a gradual drop in oxyhemoglobin concentration, resulting in a decrease of 5.3% over 45s, and a gradual rise in deoxyhemoglobin by 20.1% due to venous pooling and tissue metabolism. Upon release, oxyhemoglobin increases rapidly during a reactive hyperemia phase, while deoxyhemoglobin decreases resulting from re-established venous return. These observations were consistent with previously reported occlusion results using a contact-based diffuse reflectance spectroscopy system [4].

## 4. Discussion

As demonstrated, the multispectral imaging system was able to simultaneously acquire three, stably illuminated videos. For the light intensity analysis, both the local fluctuations (current-driven) and overall change (thermally-driven) in the brightness are relevant, as small fluctuations in the illumination would contribute to noise in the signals obtained from videos captured by this device. A minor overall increase in intensity was observed across all the light sources, where the greatest change over the 10 mins was by 3.1 intensity units (Fig. 2). Although the observed increase was relatively small, knowledge of the thermal characteristics of the LED output is an important consideration for applications requiring greater accuracy in reflectance data. However, local fluctuations remained consistent, where the maximally observed standard deviation in intensity was 0.407 (less than 1 pixel intensity unit).

In the preliminary arterial occlusion study, quantifiable relative changes in absorbance due to oxy- and deoxyhemoglobin were observed consistent with reported changes in hemoglobin concentration in a previous cuff occlusion experiment [4]. Physiologically, the gradual increase in oxy- and decrease in deoxyhemoglobin after the start of occlusion correspond to continued capillary gas exchange and tissue metabolism. The observed sharp rise and fall in oxy- and deoxyhemoglobin respectively correspond to a reactive hyperemia event, whereby the expansion of blood vessels in response to tissue ischemia reduces vascular resistance after the removal of occlusion [9]. These results show that the present multispectral modality of this imaging system is useful in acquiring, extracting, and analyzing relative changes in oxy- and deoxyhemoglobin absorbance consistent with physiological hemodynamic changes in the thenar eminence.

## 5. Conclusions

The design and evaluation of a multispectral biophotonic imaging system was presented. Specialized optical and electronic components allowed for simultaneous capture of multiple videos with different sources of illumination. Local deviations in light intensity given off by the optical subsystem remained under 0.5 intensity units, mitigating the light source as a source of noise in captured data. Its ability to capture changes in absorbance due to changes in oxy- and deoxyhemoglobin demonstrates its relevance to cardiovascular applications. The non-contact nature, different imaging configurations and portability made possible by the described improvements allow for imaging in a variety of applications and settings. Next steps could include combining the multispectral image acquisition with existing spatial pulsatility framework to simultaneously map blood flow and tissue oxygenation.

## Acknowledgement

This work was supported by the Natural Sciences and Engineering Research Council (NSERC) of Canada, AGE-WELL NCE Inc., and the Canada Research Chairs program.

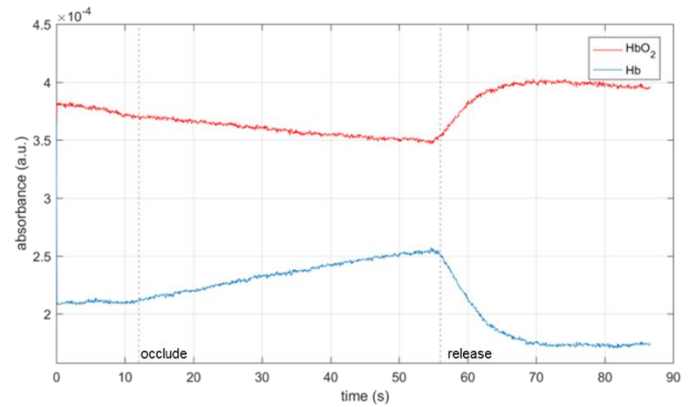


Fig. 3: Plot of chromophore absorption at the thenar eminence over time during a cuff occlusion. The dotted lines represent the start and release of the upper arm occlusion, respectively.

## References

- [1] Boyd O., Grounds R.M., and Bennett E.D. A randomized clinical trial of the effect of deliberate perioperative increase of oxygen delivery on mortality in high-risk surgical patients. *JAMA* (1993).
- [2] Belzberg, H., Wo, C.C.J., Demetriades, D., and Shoemaker, W.C. Effects of age and obesity on hemodynamics, tissue oxygenation, and outcome after trauma. *Journal of Trauma-Injury Infection & Critical Care* (2007).
- [3] Bezemer, R., et al. Simultaneous multi-depth assessment of tissue oxygen saturation in thenar and forearm using near-infrared spectroscopy during a simple cardiovascular challenge. *Critical Care* (2009).
- [4] Zonios, G., Bykowski, J., and Kollias, N. Skin melanin, hemoglobin, and light scattering properties can be quantitatively assessed *in vivo* using diffuse reflectance spectroscopy. *Journal of Investigative Dermatology* (2001).
- [5] Amelard, R., Clausi, D.A., and Wong, A. Spatial probabilistic pulsatility model for enhancing photoplethysmographic imaging systems. *Journal of Biomedical Optics* (2016).
- [6] Amelard, R., et al. Non-contact hemodynamic imaging reveals the jugular venous pulse waveform. *Nature Scientific Reports* (2017).
- [7] Wilson, M., Amelard, R., Clausi, D.A., and Wong, A. Co-integrating thermal and hemodynamic imaging for physiological monitoring. *Journal of Computational Vision and Imaging Systems* (2016).
- [8] Pellicer, A., and Bravo, M.d.C. Near-infrared spectroscopy: A methodology-focused review. *Seminars in Fetal & Neonatal Medicine* (2011).
- [9] Wood, J.E., Litter, J., and Wilkins, R.W. The mechanism of limb segment reactive hyperemia in man. *Circulation Research* (1955).